Proceedings of the 9th International Conference on Fluid Flow, Heat and Mass Transfer (FFHMT'22)
Niagara Falls, Canada – June 08-10, 2022
Paper No. 157
DOI: 10.11159/ffhmt22.157

Experimental Analysis and CFD Modelling of the Flow Conditions inside an Air-Core-Liquid-Ring Atomizer

Miguel Ballesteros[1], Volker Gaukel[1]
[1]Institute of Process Engineering in Life Sciences,
Chair of Food Process Engineering, Karlsruhe Institute of Technology
Kaiserstraße 12, 76131 Karlsruhe, Germany
miguel.ballesteros@kit.edu; volker.gaukel@kit.edu

Abstract - The Air-Core-Liquid-Ring (ACLR) atomization is an innovative internal-mixing pneumatic atomization technique, suitable for energy-efficient spray drying because of its ability to handle highly viscous liquid feeds with high solid contents. However, pneumatic atomizers such as the ACLR can suffer from unstable internal flow conditions, which may lead to a wide variation in the droplet diameter obtained. Therefore, the internal flow conditions of an ACLR-atomizer prototype needed to be studied and comprehended. With that in mind, a computational fluid dynamic (CFD) model was developed, and tested with experimental data collected for different gas pressures and liquid feed viscosities. A mesh independence study, as well as some testing of Physics models were performed. A mixed polyhedral – prismatic mesh was generated, and the k-ω SST model was selected as it showed a good balance between representation of the turbulence in the system and computational effort. The predicted average lamella thickness is similar with experimental results, with an average 10 % error, but the thickness variations observed in the experiments dampen quickly over time in the simulations. This is not the case in the experiments with the higher viscous maltodextrin solution. Therefore, further model refining has still to be done. Nonetheless, the flow behaves as expected in the CFD simulation with changes in pressure and liquid viscosity. This opens up the possibilities of doing more in-detail CFD studies of the effect of liquid feed properties and geometrical variations of the nozzle.

Keywords**:** Air-Core-Liquid-Ring (ACLR) Nozzle; CFD; Multiphase Flow; Annular Flow; Atomization

1. Introduction

Liquid atomization is an essential process operation that used in different industrial processes such as surface coating, combustion, or spray drying. Increasing the surface area of a liquid requires energy, which must be transferred to the liquid flow using a suitable atomizer [1]. Due to the wide range of applications, there is a vast number of different types of atomizers, each with their own strengths and weaknesses.

This particular study focused on understanding the behaviour and performance of the Air-Core-Liquid-Ring (ACLR) nozzle, which is a type of internal-mixing pneumatic nozzle. A scheme of the nozzle is shown in Fig. 1. The device is composed of two concentric tubes. The outer tube is where the liquid feed flows, while a capillary at the centre carries the gas and injects it at the core of the liquid phase in the mixing chamber. This forms an annular flow, with a liquid film around the gas core. As this two-phase flow exits the nozzle, the gas phase expands, and the liquid phase breaks up in a cone that then disperses into droplets [2].

With this atomizer, highly viscous, or high solid-content, liquids can be atomized with a low energy input [3]. However, as with most internal-mixing pneumatic nozzle, the free-surface interaction between the gas and the liquid inside the nozzle causes the flow conditions to be unstable and highly turbulent, which may lead to a wide variation in the droplet diameter obtained during atomization [4]. Therefore, the internal flow of an ACLR-atomizer prototype needs to be fully comprehended. This knowledge is essential to formulate the process function of the ACLR nozzle and then be able to tailor the nozzle design for specific industrial applications.

Since it is not feasible to measure pressure and velocity profiles inside the nozzle, this study focused on developing a Computational Fluid Dynamics (CFD) model that can allow us to investigate the fluid behaviour inside the ACLR-atomizer, provide information on various flow variables, and predict the effect of different process conditions. A developed

model could be used to analyse the relation between nozzle geometry and nozzle performance, which would enable the aforementioned tailored design for a specific industrial application.

While there are some computational studies of pneumatic internal-mixing models, most of them modelled only water-air mixtures or did very limited experimental validation of the model [5, 6]. Only Wittner et al. [7] focused on the ACLR nozzle design. However, they assumed a constant density for the gas phase, instead of using a compressible gas model, which can increase simulation error [5]. The purpose of this study was therefore to develop an efficient and reliable CFD model that could accurately represent the flow conditions inside the ACLR nozzle, and to validate this model with experimental data with a high-viscosity fluid, since it is the main application of this type of nozzle.

2. Materials and Methods

The study involved extensive mesh and physics models testing, to develop a CFD model that accurately represented the physical system. An experimental validation was performed, to evaluate the accuracy of the computational predictions. ANSYS Fluent 2019 was used for the simulations, while the experiments were performed on a modular spray test rig [7].

2.1. Nozzle Design and Mesh Generation

The ACLR nozzle that was investigated in the simulations and experiments is displayed on the left of Fig. 1. It consists of two parts: a metal capillary tube, which injects the compressed gas, and a clear acrylic block around it that receives the liquid feed and houses the mixing chamber (with a length of 2.4 mm) and the outlet channel (with a length and diameter of 1.5 mm). The clear acrylic was chosen because it allowed direct observation of the interior annular flow. On the other hand, the right of Fig. 1 shows the mesh that was used to represent the system.

Since the aim of the study was to understand the two-phase flow inside the nozzle, the mixing chamber and outlet channels were designated as the main regions of interest and were meshed with a polyhedral grid, as seen on Fig. 1-C. This type of grid was chosen because it can form uniform multi-faceted cells all along geometry, where each cell is connected to a high number of neighbours. This generates a better and more robust approximation of transport gradients [8]. It should be noted that thin prismatic cells were generated near the wall to better approximate the boundary layer [9]. Polyhedral grids tend to have a high density of cells, so the inlet regions (i.e. the liquid feed ring and the gas capillary) were meshed with a coarser prismatic grid (see Fig. 1-B) that was extruded from the regions of interests, so that the polyhedral and prismatic meshes would match.

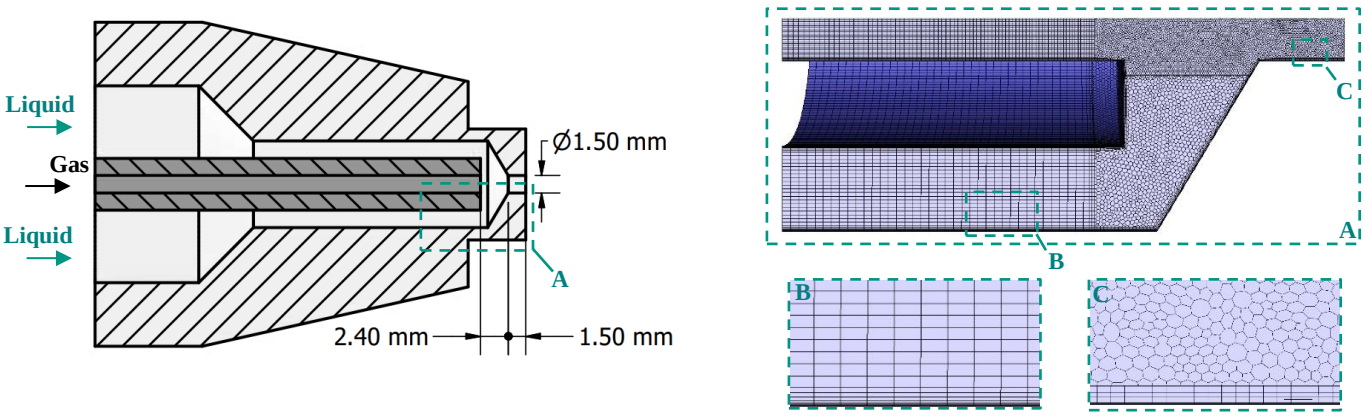

Fig. 1: Left: Nozzle geometry, which is composed of a steel capillary (dark grey), and a PMMA block (light grey). Right: Mesh representation of the quarter of the nozzle that was simulated. The general meshed region is shown on A, with some close-up to the two types of mesh used: extruded prismatic cells (B) and a polyhedral grid (C).

In order to reduce computation cost, especially for the mesh and model testing, only a quarter of the nozzle was simulated. This type of simplification is common in multiphase computational analysis. Many studies with segregated and annular flows assume bilateral or even axi-symmetry [5, 10] in inclined and vertical flows. It is important to note that the

simplification does not mean that each quarter of the nozzle behaves exactly the same, but rather that there is no consistent difference between each quarter of the nozzle. That means, though there may be local and temporal differences and perturbations in the flow on each side, the nozzle average behaviour can still be deduced from modelling a quarter of it. In result, the reduction of computational cost allows the CFD model to be more easily and efficiently applied for further analysis.

2.2. Experimental Validation and Operating Conditions

The experimental measurements were carried out at a modular spray test rig, using the methodology and experimental setup mentioned by Wittner et al. [7]. This setup consisted, in essence, of a high-speed camera (OS3-V3-S3, Integrated Design Tools Inc., Tallahassee, FL, USA), which captured the flow inside the nozzle, and a MATLAB code that tracked the gas-liquid interface by analysing the greyscale values in each image. However, as mentioned by previous researchers [7, 11], refraction inside the nozzle could distort dimension measurements inside the nozzle or hinder the interface recognition, particularly for very low film thicknesses. These refraction errors were evaluated with ray-tracing theoretical calculations, which led to the conclusion that distortions in thickness measurement were corrected by the calibration. Recognition errors could be reduced by adjusting the code sensibility in the near-wall regions.

Experiments were carried out with water and with a 47% w/w maltodextrin solution (Cargill C*DryTM MD 01910, Germany). A liquid volume flow of 40 L/h was ensured for all measurements by an eccentric screw pump (NM011BY, Erich Netzsch GmbH and Co. Holding KG, Germany). The atomizing gas was compressed air, and the pressure was varied for different measurements. The validation of the CFD model was performed using both water and maltodextrin solution, and with two different pressures (0.2 and 0.4 MPa), in order to cover a wide range of operating conditions. The properties of the fluids can be seen in Table 1, though the gas properties are average, since they change with operating pressure.

Table 1: Average properties of the simulated phases

Phase	Density (kg/m^3)	Viscosity ($Pa \cdot s$)	Surface Tension (N/m)
Maltodextrin solution	1234	0.14	0.049
Water	997	1×10^{-3}	0.074
Compressed air	6	1.8×10^{-5}	-

It should be noted that, just as in the experimental setup, the gas pressure and the liquid flow were the inlet boundary conditions set in the simulations. The nozzle exit was set as atmospheric pressure outlet, while two symmetry planes were set in the faces where the nozzle was divided into quarters. As for the initialization, the mixing chamber and the liquid feed ring were set as filled with liquid, while the capillary and outlet channel were initialized as filled with gas.

2.3. Numerical Model Development and Testing

The flow inside the nozzle was modelled as an immiscible mixture of the two phases. The liquid phase was incompressible and Newtonian, while three different equations-of-state were tested for the gas phase (incompressible, ideal gas, and the Redlich-Kwong model for a real gas [12]). The multiphase flow was simulated using the Volume Of Fluid (VOF) method. This model assumes that all fluid phases share the same pressure and velocity fields. This means that the two-phase system is modelled as a single-phase fluid, whose physical properties are calculated from the volume averages of the properties of the actual phases [13]. This method requires the introduction of an additional differential transport equation for the volume fraction of the phases, which can be solved using different schemes.

Geometric schemes, such as Geo-Reconstruct, track the discontinuities in the volume fraction field and reconstruct a sharp interface between the gas and the liquid, but they can be very computationally expensive [14]. On the other hand, compressive methods, such as CICSAM and HRIC skip the explicit geometrical reconstruction of the interface, which makes them more efficient, but can lead to a diffuse or distorted interface [15]. It was therefore necessary to test which scheme worked better when simulating the annular flow inside the nozzle. Along the gas-liquid interface, the fluid

immiscibility generates a tensile tangential force known as surface tension force. This force is modelled by the VOF method using the Continuum Surface Method (CSF) developed by Brackbill et al. [16].

As it is a high-Reynolds flow, a turbulence model had to be selected. Four options were evaluated, based on accuracy and computational cost. The first two, the k – ω SST and the k – ϵ turbulence viscosity models, are fairly similar: both are computationally efficient and consist of sets of two transport equations that model the energy dissipation caused by the turbulent vortices. Then, there is the Reynolds Stress Model (RSM), which uses a set of seven equations. This causes the model to be quite computationally expensive, but it can simulate anisotropic and rotational phenomena that cannot be modelled with the previous models. Finally, we considered using Large Eddy Simulation (LES) model. This method directly simulates large-scale turbulence, while using the modelling approach for the smaller-scale eddies [17].

The mesh and physics model tests were performed using a base CFD model, which initially used the k-ω SST turbulence model, the Geo-Reconstruct scheme for interface capturing, and the ideal gas equation-of-state. These testing simulations were run with an air pressure of 0.3 MPa and a maltodextrin solution of 0.39 Pa·s, based on previous testing with the spray rig [7]. First, the mesh independence was evaluated using this base model, to determine the ideal mesh fineness. Second, the four possible turbulence models were tested, while maintaining the rest of the CFD model unaltered. The base model was then updated with the selected turbulence model, before using it to determine the interface scheme. This process was repeated once more in order to choose a gas equations-of-state. The model configuration that resulted from this step-by-step analysis was then used for the experimental validation.

3. Results and Discussion

As mentioned before, the project was divided into an experimental and a computational study. Since the focus was to develop a model for the internal flow conditions of the ACLR nozzle, all tests and evaluations from both parts of the project centred on the liquid film thickness. On the one hand, the experiments focused on refining the measurement of said lamella thickness. On the other, a mesh independence test and a physics model analysis were performed, in order to create the computational model that most accurately predicted how the liquid film would behave. Finally, the results from both experiments and simulation were compared, both to validate the CFD model and to analyse how the internal flow conditions change with different operating conditions.

3.1. Experimental Liquid Film Thickness Measurement

The liquid film thickness was measured for water and a maltodextrin solution under different operating pressures, as it can be seen on Fig. 2. As observed in previous studies [7], the film thickness varies significantly during the atomization, and the range of variation seems to become smaller as the operating pressure increases. Complete gas core breakups (points in which the whole nozzle fills with liquid) are also less frequent with higher pressure, which can be seen in Fig. 2 as the measurements that reach the value of the nozzle radius. The measurement distribution is also noticeably skewed, as there is a wider range of points above the median, than there is below. This skewedness was mostly expected from the inherent waviness of the annular flow pattern, but it is also caused in part by the difficulty of accurately measuring a film thickness below 0.05 mm, since the interface becomes obscured by the channel's curvature. This darker edge region can be seen in the photo on Fig. 5-A, marked with the green dashed rectangle. This shadow introduces some error in the code that analyses the high-speed images, since it relies on the brightness gradient to track the interface. However, this error would only become significant when the median approaches the lower limit [18], which should not happen for the high-viscosity liquids and low-to-medium operating pressures for which the ACLR nozzle is designed.

As expected, higher viscosities lead to a larger median liquid film thickness, a larger range of thickness variation, and more frequent gas core breakups. It is interesting to note, that the characteristic values for the distribution of the liquid film thickness do not change proportionally with viscosity and pressure. The median thickness for both liquids decreased around 30 % when doubling the pressure, but the $x_{95,0}$ percentile decreased twice as much for water than for the maltodextrin solution. Based on the measured distributions from Fig. 2, the aforementioned lower frequency of gas core breakups may be largely responsible, but the fact that this decrease happens for water and not the maltodextrin solution may indicate that liquids properties play a role on flow behaviour beyond just increasing the lamella thickness. Therefore, a

more in detail study of the behaviour of the nozzle with a wide range of liquid properties should be carried out in the future.

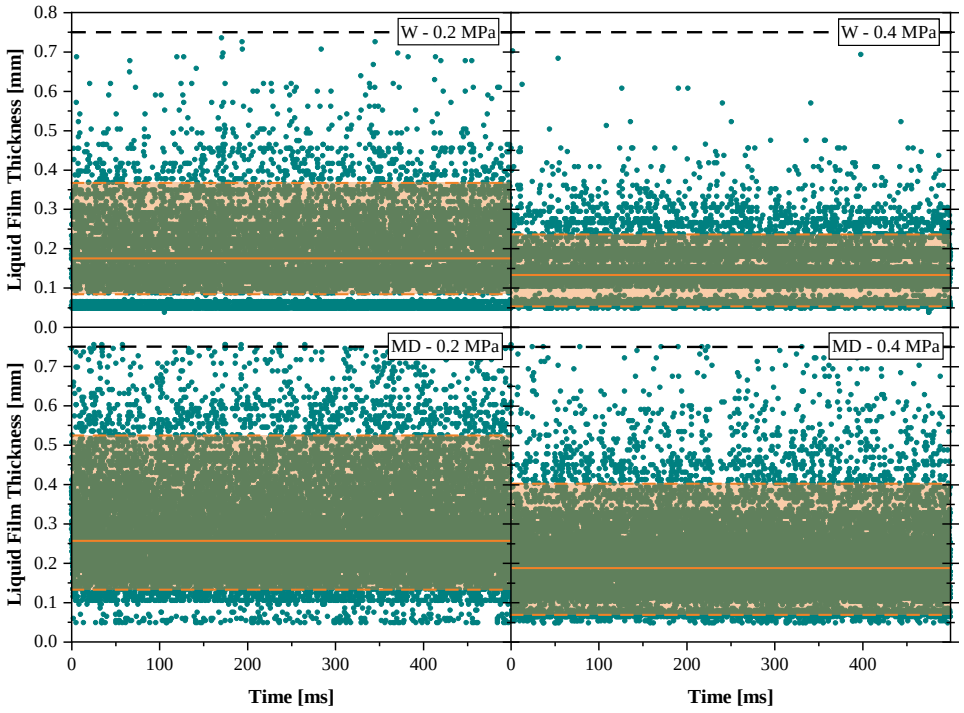

Fig. 2: Liquid film thickness for water (W) and a maltodextrin solution (MD), with a viscosity of 0.14 Pa·s, at different gas pressures and liquid flow of 40 L/h, during 0.5 s of atomization. Additionally, the percentiles $x_{5,0}$ (lower orange dashed line), $x_{50,0}$ (solid orange line) and $x_{95,0}$ (upper orange dashed line) of the liquid film thickness are given for each plot. The nozzle radius is represented as a dashed black line; a film thickness of this value means the nozzle outlet is filled completely with liquid.

3.2. Mesh Independence Test

In a mesh independence test, several simulations of the same system, with equal geometry, conditions, and physics models, are run with different mesh densities, i.e. number of cells [19] . With that in mind, the nozzle was simulated with different mesh densities and with two different fluids: water and the maltodextrin solution with 0.39 Pa·s. The average required computational time required for each mesh was also recorded. The results are shown in Fig. 3.

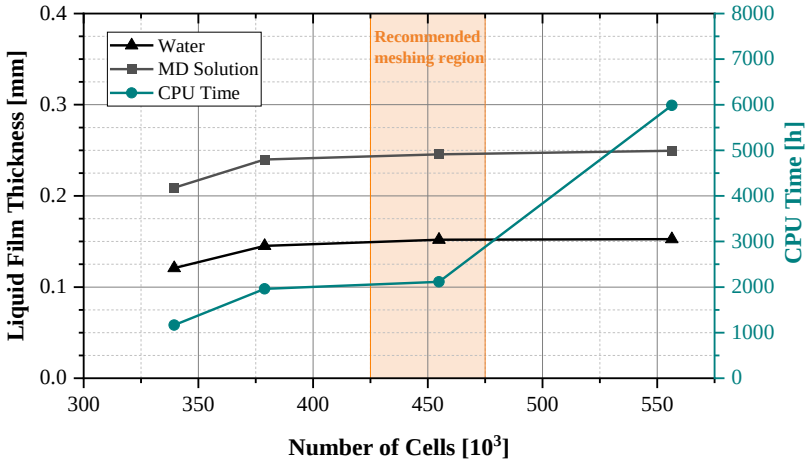

Fig. 3: Effect of the number of grid cells on predicted liquid film thickness and required simulation time, when a quarter of the ACLR nozzle is simulated with a maltodextrin solution (of 0.39 Pa·s) and with water, at a gas pressure of 0.3 MPa and liquid flow of 40 L/h.

Based on the results, we concluded that a mesh of around 450 thousand cells is appropriate to simulate a quarter of the nozzle, since it introduces no additional numerical error to the computational model. The change in the predicted film thickness is below 1 % beyond this mesh density. The relation of numerical error and mesh density is supposed to be inversely proportional [19], so it was expected that the simulated variables converged to a stable value once a certain mesh fineness was surpassed. Refining the mesh beyond this point serves no purpose, since it does not affect simulation results and only increases computational time. Additionally, since the mesh converged similarly for different liquid viscosities, the mesh should work for a wide range of operating conditions and liquid feeds as well, thereby increasing the reliability of the model.

3.3. Physics Model Analysis

The development of the CFD model was divided into three critical selection steps: turbulence modelling, interface capturing scheme, and gas equation-of-state. For turbulence modelling four models were evaluated: k–ω SST**,** k–ε**,** RSM and LES. For that effect, simulations were run with each model until the film thickness stabilized, which is shown in Fig. 4. This stabilization, which did not occur in the experimental results (see Fig. 2.), will be discussed with mayor detail in the experimental validation (see Chapter 3.4).

All models predicted similar values for liquid film thickness when they stabilized, and they all converged to values within 10 % of each other, although the behaviour during the stabilization was quite different. The RSM and LES models stabilized quickly and with very little overshoot. In contrast, the two turbulence viscosity models took a lot more time to converge, and the k-ω SST simulation particularly presented a large amount of variation after initialization. However, as we mentioned, the stabilization was a point of contention, since it was not observed in the experiments, so the difference in the behaviour right after initializing was disregarded, and only the converged value was taken into account. With that in mind, all four models performed similarly.

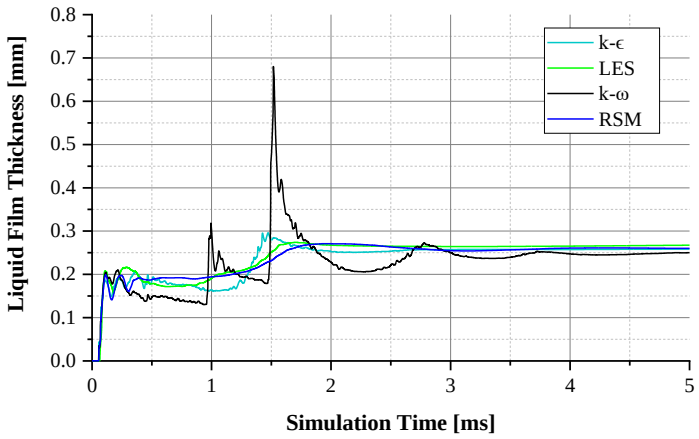

Fig. 4: Effect of the turbulence model choice on the predicted liquid film thickness when a quarter of the ACLR nozzle is simulated with a maltodextrin solution (of 0.39 Pa·s) and with water, at a gas pressure of 0.3 MPa and liquid flow of 40 L/h.

This meant that the choice had to be based on the computational efficiency of each model instead. RSM and LES were much more computationally expensive than the turbulence viscosity (k–ω SST and k–ε) models, running at about only 25 % of their velocity, though they predicted a similar liquid film thickness. On the other hand, the two turbulence viscosity models both required similar computational times and predicted similar values. Each model also has its own advantages: the k – ω models can model the viscous regions near the channel wall with good accuracy, while k – ϵ models are more robust with respect to inlet condition parameters [20]. As it happens, the k-ω SST already uses a combination of

both models. It implements the k-ε method in the free-stream region and the k-ω method for the flow near the wall, combining the advantages of both methods [21]. Therefore, it was chosen as the most appropriate turbulence model for the CFD model.

After an appropriate turbulence model was determined, we proceeded to evaluate the most suitable interface-capturing scheme. Two different methods were tested: a geometric method: Geo-Reconstruct, and a compressive method: CICSAM. This pre-selection was based on previous studies on multiphase flow simulation, particularly for high-viscosity liquids [22, 23]. The same comparison as with the turbulence models was performed, and it was determined that the two methods produced similar results. The CICSAM method was therefore chosen, since it requires less computational effort.

Finally, three different equations-of-state for the gas phase were evaluated: a constant-density (incompressible) gas, an ideal (compressible) gas and a real gas model (Soave-Redlich-Kwong). The real gas model required about 150 % more time to run than the other options, but it still provided the same results than the ideal gas. In addition, it required multiple attempts to converge, so we discarded it. With that in mind, the incompressible and ideal gas models were compared recreating the experimental conditions from Wittner et al. [7], for the 0.39-Pa·s maltodextrin solution. Surprisingly, the incompressible gas phase model did not present the artificial stabilization that occurred with the ideal gas (such as the one shown on Fig. 4), instead it presented a flow variation similar to the one observed in the experiments. However, the average simulation error was larger for the incompressible model (with a difference of 15% compared to experimental data), while the ideal gas model provided an error as low as 5%. Moreover, assuming gas incompressibility is normally only considered valid with gas velocities of less than 0.3 Mach [24], which is not the case for a pneumatic nozzle such as this one. This makes the ideal-gas model a more suitable and reliable option, which is why it was chosen.

3.4. Experimental Validation of Simulated Flow Behaviour

The difference between the moment-by-moment and the average flow behaviours inside the simulated nozzles led to a more thorough comparison of simulation and experimental results. For this purpose, we simulated the four operating conditions of the experimental measurements shown in chapter 3.1 (see Fig. 2). The most evident difference with the experiments is that the simulation does not consistently capture flow instabilities for the simulations with maltodextrin as seen on Fig. 4. However, Fig. 5-C shows the film thickness profile when atomizing water at 0.2 MPa, both for the experiments and the simulation. It is obvious that with a less viscous fluid, such as water, the simulated flow does indeed vary along time in a manner comparable to the experiments. In this case, the core breakup (whether complete or partial) happened repeatedly along the simulation. Additionally, similar liquid profiles could be observed in the simulations and experiments during stable annular flow (Fig. 5-A) and during a gas core break up (Fig. 5-B), in which the liquid from the mixing chamber collapses and temporally fills the nozzle, trapping some bubbles between the liquid and the nozzle wall. These bubbles are marked as dashed orange rectangles in the figure.

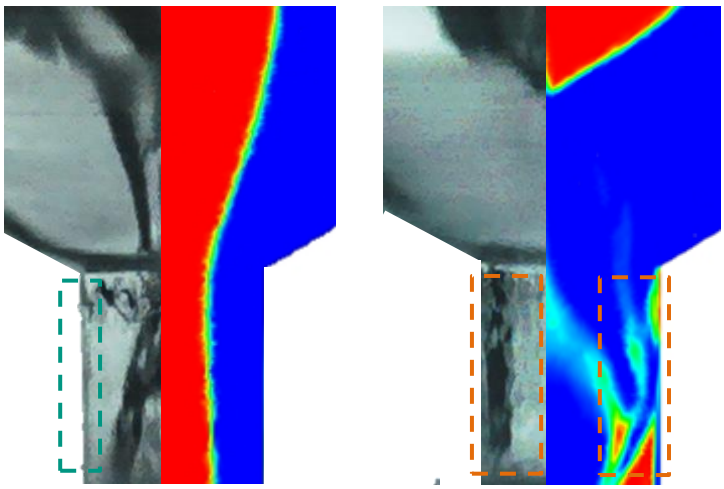

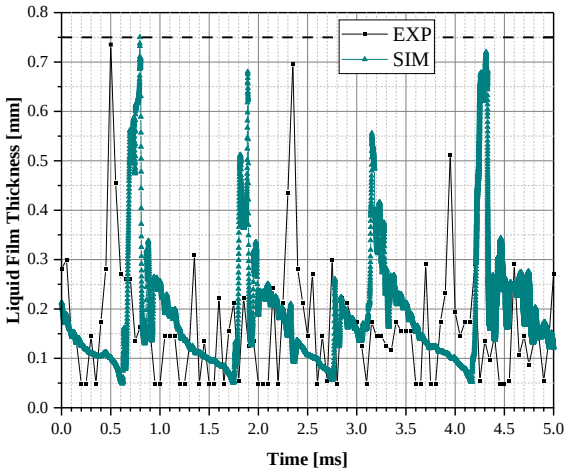

(A) (B) (C)

Fig. 5: (A) Stable liquid profile in experiments (left) and simulations (right). (B) Liquid profile when the gas core breaks up, in experiments (left) and simulations (right). In all simulated profiles, the liquid phase is blue, while the gas is red. (C) Liquid film thickness during 5 ms of atomization for water at 0.2 MPa and with liquid flow of 40 L/h, both in experiments and in simulations. The nozzle radius is represented as a dashed black line; a film thickness of this value means the nozzle outlet is filled up with liquid.

Although the large differences between simulation and experiment with maltodextrin solutions concerning the instabilities, we compared the median liquid film thickness from simulations with the experimental results, as can be seen in Table 2. The average behaviour of the flow seems to be predicted fairly well, with a maximum relative error of less than 15 %. This is valid even with the maltodextrin simulations, in which the flow artificially stabilized. This fact led to the conclusion the CFD model may be over-averaging the flow instabilities inside the nozzle, dampening their variation over time. A time step of 0.2 µs had been selected for the simulations to ensure that no perturbation in the system advances through more than a cell in each time step, which should ensure a Courant-Friedrich-Levy number below 1 and allow proper capturing of flow variations [19]. However, the explicit discretization of the VOF method might make the model more sensitive to time discretization than expected [25]. This further indicates that the model still requires some refinement. The next step for future investigations is then to analyse the effect of time discretization. Nevertheless, it is not yet completely clear how this would relate to the fact that the artificial flow stabilization is only observed for higher liquid viscosities. It might well be, that the higher viscosity dampens the already under-calculated turbulences and instabilities in the gas phase, leading to the stable flow. For fluids like water, where the viscous forces are significantly smaller, this dampening would happen to a much lower extent.

Table 2: Median film thickness for simulations and experiments at different conditions.

Liquid	Pressure (MPa)	Experiments (mm)	Simulations (mm)	Relative error (%)
Maltodextrin solution	0.2	0.26	0.27	7
	0.4	0.19	0.18	3
Water	0.2	0.17	0.18	2
	0.4	0.13	0.11	14

4. Conclusion

A CFD model was developed to simulate the internal flow conditions of an ACLR nozzle. A mixed unstructured mesh, with both polyhedral and prismatic cells, was developed, as well as a preliminary Physics model that could represent the average behaviour of the system. The performance of this CFD model was successfully tested with experimental results. This testing proved that the behaviour of the flow inside the nozzle behaved as expected with changes in operating conditions. The liquid film thickness of the annular flow increased with the liquid viscosity and decreased with gas pressure.

The experimental measurements revealed that an increase in film thickness was also related with more flow instability, i.e. more flow variation, and more frequents gas core breakups, where the nozzle fills with liquid. The way in which these variables change indicates that there may be a flow pattern transition inside the nozzle that happens at different pressures according to liquid viscosity, which suggests that a wider range of liquids should be investigated in future.

On the other hand, the computational model cannot yet capture the temporal instabilities observed in the experimental flow, although this issue tends to happen only for liquids with higher viscosities. This indicates that further refinement is required. The next step will be to study the effect of the time discretization in the simulation and its relation with the artificial stabilization of the flow behaviour.

Acknowledgements

The authors would like to thank all previous researchers that have worked on this topic, such as Dr. Marc Wittner, and Mr. Felix Ellwanger, as well as the support by the state of Baden-Württemberg through access to the bwHPC.

References

[1] A. H. Lefebvre and V. G. McDonell, *Atomization and sprays*. Boca Raton, London, New York: CRC Press, 2017. [Online]. Available: http://www.crcnetbase.com/doi/book/10.1201/9781315120911

[2] M. O. Wittner, H. P. Karbstein, and V. Gaukel, "Spray performance and steadiness of an effervescent atomizer and an air-core-liquid-ring atomizer for application in spray drying processes of highly concentrated feeds," *Chemical Engineering and Processing - Process Intensification*, vol. 128, pp. 96–102, 2018, doi: 10.1016/j.cep.2018.04.017.

[3] P. Stähle, V. Gaukel, and H. P. Schuchmann, "Comparison of an Effervescent Nozzle and a Proposed Air-Core-Liquid-Ring (ACLR) Nozzle for Atomization of Viscous Food Liquids at Low Air Consumption," *Journal of Food Process Engineering*, vol. 40, no. 1, e12268, 2017, doi: 10.1111/jfpe.12268.

[4] M. Zaremba, L. Weiß, M. Malý, M. Wensing, J. Jedelský, and M. Jícha, "Low-pressure twin-fluid atomization: Effect of mixing process on spray formation," *International Journal of Multiphase Flow*, vol. 89, pp. 277–289, 2017, doi: 10.1016/j.ijmultiphaseflow.2016.10.015.

[5] Z. Alizadeh Kaklar and M. R. Ansari, "Numerical analysis of the internal flow and the mixing chamber length effects on the liquid film thickness exiting from the effervescent atomizer," *J Therm Anal Calorim*, vol. 135, no. 3, pp. 1881–1890, 2019, doi: 10.1007/s10973-018-7485-3.

[6] M. Mousavi and A. Dolatabadi, "Numerical study of the effect of gas-to-liquid ratio on the internal and external flows of effervescent atomizers," vol. 42, no. 4, pp. 444–456, 2018, doi: 10.1139/tcsme-2017-0125.

[7] M. O. Wittner, M. A. Ballesteros, F. J. Link, H. P. Karbstein, and V. Gaukel, "Air-Core–Liquid-Ring (ACLR) Atomization Part II: Influence of Process Parameters on the Stability of Internal Liquid Film Thickness and Resulting Spray Droplet Sizes," *Processes*, vol. 7, no. 9, p. 616, 2019, doi: 10.3390/pr7090616.

[8] M. Sosnowski, J. Krzywanski, and R. Gnatowska, "Polyhedral meshing as an innovative approach to computational domain discretization of a cyclone in a fluidized bed CLC unit," *E3S Web Conf.*, vol. 14, p. 1027, 2017, doi: 10.1051/e3sconf/20171401027.

[9] K. Okumura, "CFD Simulation by Automatically Generated Tetrahedral and Prismatic Cells for Engine Intake Duct and Coolant Flow in Three Days," in *SAE Technical Paper Series*, 2000.

[10] M. Ballesteros Martínez, E. Pereyra, and N. Ratkovich, "CFD study and experimental validation of low liquid-loading flow assurance in oil and gas transport: studying the effect of fluid properties and operating conditions on flow variables," *Heliyon*, vol. 6, no. 12, e05705, 2020, doi: 10.1016/j.heliyon.2020.e05705.

[11] M. Maly, J. Jedelsky, J. Slama, L. Janackova, M. Sapik, G. Wigley and M. Jicha, "Internal flow and air core dynamics in Simplex and Spill-return pressure-swirl atomizers," *International Journal of Heat and Mass Transfer*, vol. 123, pp. 805–814, 2018, doi: 10.1016/j.ijheatmasstransfer.2018.02.090.

[12] R. H. Aungier, "A Fast, Accurate Real Gas Equation of State for Fluid Dynamic Analysis Applications," *Journal of Fluids Engineering*, vol. 117, no. 2, pp. 277–281, 1995, doi: 10.1115/1.2817141.

[13] S. Sun and T. Zhang, "Review of classical reservoir simulation," in *Reservoir Simulations*: Elsevier, 2020, pp. 23–86.

[14] F. Denner and B. G. van Wachem, "Compressive VOF method with skewness correction to capture sharp interfaces on arbitrary meshes," *Journal of Computational Physics*, vol. 279, pp. 127–144, 2014, doi: 10.1016/j.jcp.2014.09.002.

[15] Di Zhang, C. Jiang, D. Liang, Z. Chen, Y. Yang, and Y. Shi, "A refined volume-of-fluid algorithm for capturing sharp fluid interfaces on arbitrary meshes," *Journal of Computational Physics*, vol. 274, pp. 709–736, 2014, doi: 10.1016/j.jcp.2014.06.043.

[16] J. Brackbill, D. Kothe, and C. Zemach, “A continuum method for modeling surface tension,” *Journal of Computational Physics*, vol. 100, no. 2, pp. 335–354, 1992, doi: 10.1016/0021-9991(92)90240-Y.
[17] C. Baker, T. Johnson, D. Flynn, H. Hemida, A. Quinn, D. Soper and M. Sterling, “Computational techniques,” in *Train Aerodynamics*: Elsevier, 2019, pp. 53–71.
[18] F. P. Hartwig, G. Davey Smith, A. F. Schmidt, J. A. C. Sterne, J. P. T. Higgins, and J. Bowden, “The median and the mode as robust meta-analysis estimators in the presence of small-study effects and outliers,” *Research synthesis methods*, vol. 11, no. 3, pp. 397–412, 2020, doi: 10.1002/jrsm.1402.
[19] H. K. Versteeg and W. Malalasekera, *An introduction to computational fluid dynamics: The finite volume method*, 2nd ed. Harlow: Pearson/Prentice Hall, 2007.
[20] F. R. Menter, “Improved two-equation k-omega turbulence models for aerodynamic flows,” *NASA STI/Recon Technical Report N*, vol. 93, p. 22809, 1992.
[21] P. Zahedi, J. Zhang, H. Arabnejad, B. S. McLaury, and S. A. Shirazi, “CFD simulation of multiphase flows and erosion predictions under annular flow and low liquid loading conditions,” *Wear*, 376-377, pp. 1260–1270, 2017, doi: 10.1016/j.wear.2017.01.111.
[22] M. Jabbari, R. Bulatova, J. H. Hattel, and C. Bahl, “An evaluation of interface capturing methods in a VOF based model for multiphase flow of a non-Newtonian ceramic in tape casting,” *Applied Mathematical Modelling*, vol. 38, no. 13, pp. 3222–3232, 2014, doi: 10.1016/j.apm.2013.11.046.
[23] T. Waclawczyk and T. Koronowicz, “Comparison of CICSAM and HRIC high-resolution schemes for interface capturing,” *Journal of Theoretical and Applied Mechanics*, vol. 46, no. 2, pp. 325–345, 2008.
[24] J. D. Anderson, *Fundamentals of aerodynamics*. New York, NY: McGraw-Hill Education, 2017.
[25] T. Pulliam, “Time accuracy and the use of implicit methods,” in *11th Computational Fluid Dynamics Conference*, Orlando,FL,U.S.A, 1993.